Monthly Notices
of the
ROYAL ASTRONOMICAL SOCIETY

Mon. Not. R. Astron. Soc. **421,** 3538–3542 (2012) doi:10.1111/j.1365-2966.2012.20570.x

Suzaku study of the centrally brightened supernova remnant G272.2−3.2

A. Sezer[1,2]★ and F. Gök[3]★

[1]*TÜBİTAK Space Technologies Research Institute, ODTU Campus, Ankara 06531, Turkey*
[2]*Boğaziçi University, Faculty of Art and Sciences, Department of Physics, Istanbul 34342, Turkey*
[3]*Akdeniz University, Faculty of Sciences, Department of Physics, Antalya 07058, Turkey*

Accepted 2012 January 16. Received 2012 January 9; in original form 2011 November 3

ABSTRACT

In this paper, we present the results from a *Suzaku* observation of the Galactic supernova remnant G272.2−3.2. The spectra of G272.2−3.2 are well fitted by a single-temperature variable abundance non-equilibrium ionization (VNEI) model with an electron temperature $kT_e \sim 0.77$ keV, an ionization time-scale $\tau \sim 6.5 \times 10^{10}$ cm^{-3} s and an absorbing column density $N_H \sim 1.1 \times 10^{22}$ cm^{-2}. We have detected enhanced abundances of Si, S, Ca, Fe and Ni in the centre region, indicating that the X-ray emission has an ejecta origin. We estimate that the electron density is $n_e \sim 0.48 f^{-1/2}$ cm^{-3}, the age is $\sim 4300 f^{1/2}$ yr and the X-ray total mass is $M_x = 475 f^{1/2}$ M$_\odot$ by taking the distance to be $d = 10$ kpc. To understand the origin of the centrally peaked X-ray emission of the remnant, we have studied the radial variations of the electron temperature and surface brightness. The relative abundances in the centre region suggest that G272.2−3.2 is the result of a Type Ia supernova explosion.

Key words: ISM: individual objects: G272.2−3.2 – ISM: supernova remnants – X-rays: ISM.

1 INTRODUCTION

The Galactic supernova remnant (SNR) G272.2−3.2 was discovered in X-rays with the *ROSAT* All-Sky Survey (Greiner & Egger 1993). It has a centrally filled X-ray morphology and a thermally dominated X-ray spectrum. From the *ROSAT* Position Sensitive Proportional Counter (PSPC) data, Greiner, Egger & Aschenbach (1994) found that the electron temperature was between 1.0 and 1.5 keV. Winkler, Hanson & Phillips (1993) confirmed that the nature of the emission was shock-heated and the nebulosity was a SNR by measuring the [S II]/Hα ratio and detecting emissions from [N II] 658.3 nm and [O II] 732.5 nm in the optical band. Duncan et al. (1997) carried out a series of radio observations with the Parkes radio telescope, the Australia Telescope Compact Array (ATCA) and the Molonglo Observatory Synthesis Telescope (MOST). Using these observations, they have shown that the radio spectral index of this remnant ($\alpha \sim 0.55$) is typical of shell-type SNRs, and that it is almost circular in appearance with a diameter of ∼15 arcmin. The remnant consists of faint filaments and patches of emission with a low surface brightness, as well as bright blobs that correlate well with the brightest optical filaments. It also has a diffuse emission component produced by shock-accelerated electrons. Using *ASCA* and *ROSAT* observations, Harrus et al. (2001) found that the X-ray emission from G272.2−3.2 could best be described by a non-equilibrium ionization (NEI) model with an electron temperature of about 0.7 keV, an ionization time-scale of 3200 cm^{-3} yr and a relatively high column density, $N_H \sim 10^{22}$ atoms^{-2}. They discussed cloud evaporation and thermal conduction models to explain the centrally peaked X-ray morphology of the remnant. Later, using an X-ray study of G272.2−3.2 from *Chandra*, Park et al. (2009) reported that the X-ray spectra of the outer shell regions showed normal compositions, consistent with the shocked interstellar medium (ISM), while the central emission showed elevated abundances, suggesting reverse shocked stellar ejecta from a Type Ia supernova (SN). Based on the *Chandra* observation, Lopez et al. (2011) have confirmed that G272.2−3.2 has a Type Ia SN origin.

The distance to G272.2−3.2 is not well known. Using the observed interstellar absorption, it has been estimated to be $1.8^{+1.4}_{-0.8}$ kpc by Greiner et al. (1994). Using a statistical analysis, Harrus et al. (2001) have calculated a value of 2 kpc, which is in agreement with the distance found by Greiner et al. (1994). They have also obtained an upper limit of 10 kpc, using optical colour excess with a distance of roughly 0.2 mag kpc^{-1} in the direction of G272.2−3.2, and they have adopted an intermediate distance of 5 kpc to this remnant.

In this paper, we investigate the nature of the X-ray emission from G272.2−3.2, which is characterized by an apparent centrally brightened X-ray morphology and thermally dominated X-ray emission. We use the superior spectral capabilities for diffuse sources of the X-ray Imaging Spectrometer (XIS; Koyama et al. 2007) onboard the *Suzaku* satellite (Mitsuda et al. 2007). The structure of the paper is as follows. In Section 2, we describe the *Suzaku* observation and the data reduction. We present image and spectral analyses in Sections 3 and 4, respectively. In Section 5, we discuss the physical

★E-mail: aytap.sezer@uzay.tubitak.gov.tr (AS); gok@akdeniz.edu.tr (FG)

properties of the thermal X-ray emitting plasma (Section 5.1), the possible reasons for the centrally peaked morphology (Section 5.2) and, finally, the relative abundances in the ejecta (Section 5.3).

2 OBSERVATION AND DATA REDUCTION

Suzaku observed G272.2−3.2 on 2011 May 28 using the XIS. The observation ID and exposure time are 506060010 and 130 ks, respectively. The XIS has four CCDs: three (XIS0, XIS2 and XIS3) are front-illuminated (FI) and one (XIS1) is back-illuminated (BI). The XIS CCDs are sensitive to the 0.2–12.0 keV energy band with a 17.8 × 17.8 arcmin^2 field of view (FOV). In 2006 November, XIS2 was damaged and taken off-line. Therefore, data taken after the 2007 observation were taken only with the remaining three XIS CCDs. The XIS was operated in the normal full-frame clocking mode. Two corners of each XIS CCD have a ^{55}Fe calibration source, which can be used to calibrate the gain and to test the spectral resolution of data taken using this instrument.

Reduction and analysis of the data were performed by following the standard procedure using the HEADAS v6.4 software package, and spectral fitting was performed with XSPEC v.11.3.2 (Arnaud 1996). All of the data were reprocessed, referring to the High Energy Astrophysics Science Archive Research Center (HEASARC) calibration database (CALDB) as of 2008 July 9. The redistribution matrix files (RMFs) of the XIS were produced by XISRMFGEN, and the auxiliary response files (ARFs) by XISSIMARFGEN (Ishisaki et al. 2007).

3 IMAGE ANALYSIS

Fig. 1 shows an XIS1 image of G272.2−3.2 in the 0.3–10 keV energy band. From this figure, we see brighter emission in the central region (within ∼3.8 arcmin radius) and a relatively fainter emission in the outer part. Central and outer regions are shown by solid black circles centred at RA (2000) = $09^h06^m47^s$, Dec. (2000) = $-52^\circ06'05''$. Dashed white circles with sizes of 0–1.5, 1.5–2.5, 2.5–3.5, 3.5–4.5 and 4.5–5.5 arcmin are chosen to obtain the radial variations of the electron temperature kT_e and surface brightness. The black dashed circle with a radius of 1.5 arcmin represents the background region, RA (2000) = $09^h07^m18^s$, Dec. (2000) = $-52^\circ14'27''$, used for spectral analysis. The black dashed square indicates the FOV of the XIS1.

4 SPECTRAL ANALYSIS

The spectrum is extracted first from all over the remnant (hereafter the whole region) with a radius of 7.3 arcmin, then from the central region with the brightest X-rays and finally from the outer region, where the X-rays are fainter. This is indicated by solid black circles (see Fig. 1) for each of the XIS CCDs. The spectra are grouped with a minimum of 120 counts bin^{-1} for the whole region and 50 counts bin^{-1} for the central and outer regions.

For the whole region, we applied the VNEI model, a model in XSPEC for an NEI collisional plasma with variable abundances (Borkowski, Lyerly & Reynolds 2001), modified by interstellar absorption using cross-sections from Morrison & McCammon (1983) in the 0.3–10 keV energy range. The absorption column density N_H, the electron temperature kT_e, the ionization time-scale $\tau = n_e t$ (where n_e is the electron density and t is the elapsed time after the plasma was heated up) and the normalization were set as free parameters, and all elemental abundances were fixed to their solar values given by Anders & Grevesse (1989). From this fit, we obtained a reduced χ^2 of 1.81 for 752 degrees of freedom (dof). Then,

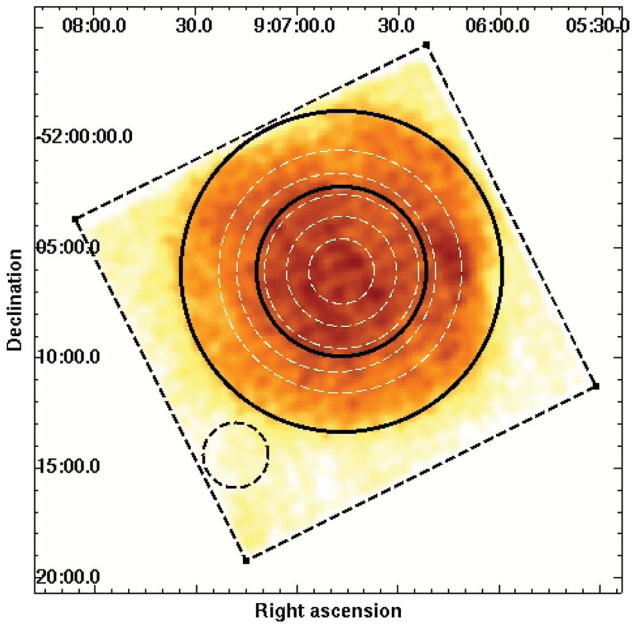

Figure 1. *Suzaku* XIS1 image of G272.2−3.2 in the 0.3–10 keV energy band. The solid black circles show the central and outer regions and the dashed white circles show the regions chosen to obtain the radial variations of the electron temperature and surface brightness. The black dashed circle represents the background region. The FOV of the XIS1 is indicated by the black dashed square. The coordinates (RA and Dec.) refer to epoch J2000.

we allowed O, Ne, Mg, Si, S and Fe abundances to vary, because these abundances appeared to differ from their solar values and the line features were evident in the spectra, while other elemental abundances were kept at their solar values. In this case, the spectral fit has significantly improved with a reduced χ^2 of 1.02 for 746 dof. We repeated the same steps for the central and outer regions. The parameter values obtained for each region are listed in Table 1, and the errors quoted are 90 per cent confidence limits. Fig. 2 shows the background-subtracted FI XIS (XIS0 and XIS3) spectra of each region in the energy range 0.3–10 keV.

Table 1. Best-fitting parameters of the spectral fitting in the 0.3–10 keV energy band for all over the remnant (whole), its centre and outer regions with an absorbed VNEI model, with corresponding errors at 90 per cent confidence level (2.7σ).

Parameters	Whole	Centre	Outer
N_H(× 10^{22} cm^{-2})	1.07 ± 0.02	1.14 ± 0.02	0.96 ± 0.02
kT_e(keV)	0.77 ± 0.02	0.83 ± 0.03	0.76 ± 0.02
O (solar)	1.4 ± 0.4	(1)	0.6 ± 0.2
Ne (solar)	0.6 ± 0.1	0.2 ± 0.1	0.4 ± 0.1
Mg (solar)	0.7 ± 0.1	0.7 ± 0.1	0.6 ± 0.1
Si (solar)	1.3 ± 0.1	2.0 ± 0.1	0.8 ± 0.1
S (solar)	2.2 ± 0.2	4.0 ± 0.2	1.2 ± 0.1
Ca (solar)	(1)	1.8 ± 1.1	(1)
Fe (solar)	1.3 ± 0.2	1.96 ± 0.11	0.8 ± 0.1
Ni (solar)	(1)	3.9 ± 0.9	(1)
$n_e t$ (× 10^{10} cm^{-3} s)	6.5 ± 0.6	5.3± 0.5	6.2± 0.6
Normalization	0.19 ± 0.02	0.17 ± 0.01	0.16± 0.01
Flux[a]	17.0 ± 0.2	6.2 ± 0.1	10.8 ± 0.1
χ^2/dof	760.7/746=1.02	917.2/686=1.34	733.7/945=0.78

[a] Flux-corrected for Galactic absorption in the 0.3–10 keV energy band in units of 10^{-10} erg s^{-1} cm^{-2}.

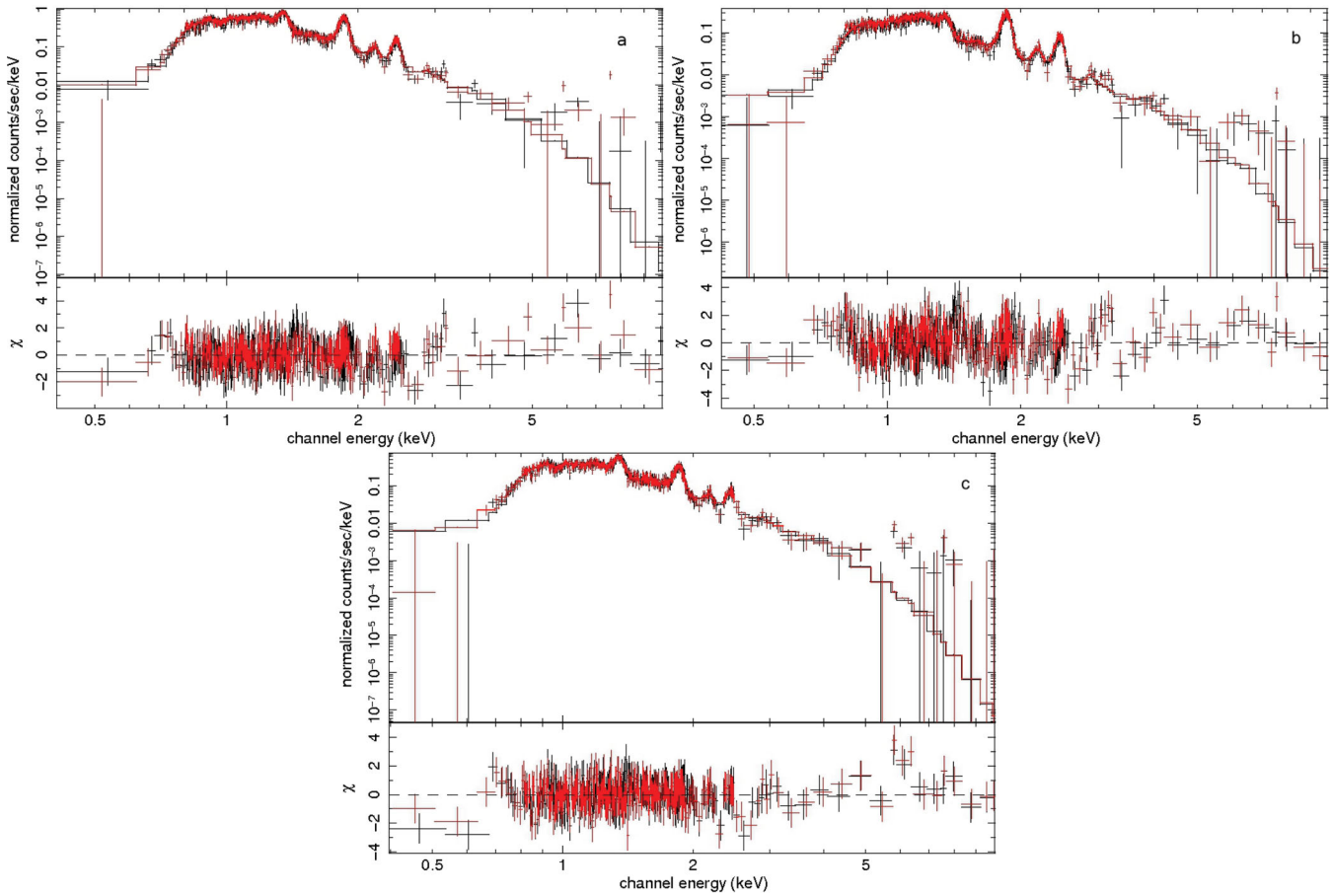

Figure 2. *Suzaku* FI (red denotes XIS0 and black denotes XIS3) spectra of G272.2−3.2 in the 0.3–10 keV energy band: (a) whole region; (b) central region; (c) outer region. The lower panels give the residuals from the best-fitting model for the FI XIS spectra.

The radial variations of the electron temperature and surface brightness are plotted in Fig. 3. During spectral fittings, in order to obtain an estimate of the possible temperature variation across the SNR, we fixed the absorbing column density and the ionization time-scale to the values of the whole region.

5 DISCUSSION AND CONCLUSIONS

In this paper, we report on the results of high-quality X-ray spectra and a detailed analysis of G272.2–3.2 using a *Suzaku* XIS observation. The X-ray spectra can be represented with a VNEI model with an electron temperature of $kT_e \sim 0.77$ keV, a high absorbing column density and a relatively small ionization time-scale, less than 10^{12} cm^{-3} s. We found clear K-shell lines of O, Ne, Mg, Si, S, Ca, Fe and Ni in the 0.3–10 keV band spectra, as shown in Fig. 2. The central region is enhanced in Si, S, Ca, Fe and Ni, as shown in Table 1. This fact suggests that the X-ray emission originating from this region results from the ejecta. The abundances of the outer region are consistent with solar values, indicating that the X-ray emission is produced by swept-up ISM. The abundances obtained from the spectra of the whole region show that the X-ray emission results from a mixture of the ejecta and ISM. This remnant shows a centrally peaked X-ray emission and extends to a radius of ∼7.3 arcmin, as seen in the XIS1 image (see Fig. 1). We discus the possible reasons for the centrally peaked emission in Section 5.2.

5.1 Thermal emission

From the thermal X-ray spectra of G272.2−3.2, we have found a high absorbing column density of $N_H \sim 1.07 \times 10^{22}$ cm^{-2}, which is in agreement with the value obtained by Harrus et al. (2001) with *ROSAT* spectral fits and with the Galactic H I column density in that direction, $N_H \sim 0.9 \times 10^{22}$ cm^{-2} (Dickey & Lockman 1990). During the analysis, we allowed N_H to vary for the whole region and the central and outer parts in order to see whether there is a significant variation all over the remnant. We have found that the N_H values obtained for these three regions are similar, which indicates that there is no significant density gradient across the remnant. Reasons for the high N_H value might be that the remnant's distance is large, or there could be molecular material or dust along the line of sight in that direction, or both. However, in the literature, no such material has yet been reported in that direction or in the vicinity of the remnant. Considering these cases, throughout our calculations, we use the upper limit distance value, $d = 10$ kpc, given by Harrus et al. (2001).

The XIS spectra suggest an ionization time-scale of $n_e t \sim 6.5 \times 10^{10}$ cm^{-3} s. For the full ionization equilibrium, the ionization time-scale, $\tau = n_e t$, is required to be $\geq 10^{12}$ cm^{-3} s (Masai 1984). The value that we have obtained for G272.2−3.2 shows that the plasma is far from the full ionization equilibrium. We have estimated the X-ray emitting plasma volume of the remnant to be $\sim 1.2 \times 10^{60} f$ cm^3, where f is the volume filling factor of the emitting gas

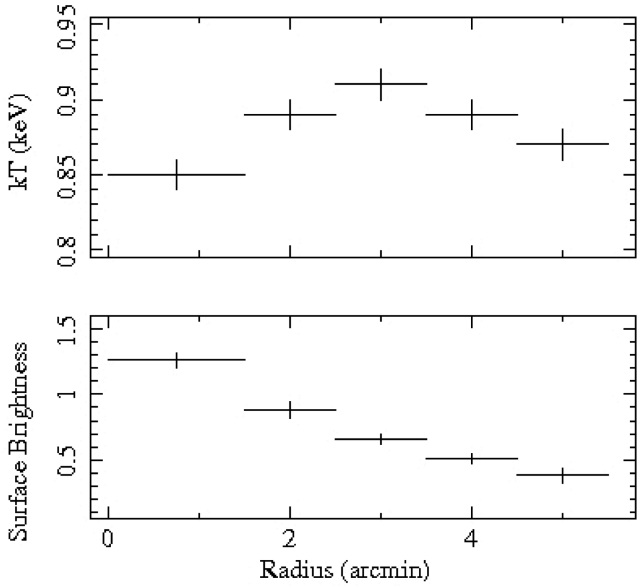

Figure 3. Radial variations of the observed electron temperature and surface brightness of G272.2−3.2. The surface brightness is in units of $(\times 10^{-11})$ erg s^{-1} cm^{-2} arcmin^{-2}.

within the SNR. We have assumed the emitting region to be a full sphere of radius 7.3 arcmin, which is our XIS spectral extraction region. Based on the emission measure $EM = n_e n_H V$, determined by the spectral fitting, where n_e and n_H are the number densities of electrons and protons, respectively, and V is the X-ray emitting volume, and assuming $n_e = 1.2n_H$, we have calculated the electron density of the plasma n_e to be $\sim 0.48 f^{-1/2}$ cm^{-3}. The age of G272.2−3.2 is calculated to be $\sim 4300 f^{1/2}$ yr from $t = \tau/n_e$. The mass of the X-ray emitting plasma of G272.2−3.2 is estimated to be $M_x = 475 f^{1/2}$ M$_\odot$ from $M_x = n_e V m_H$, where m_H is the mass of a hydrogen atom.

5.2 Radial profile

The centrally peaked X-ray morphology of G272.2−3.2 can be explained by two models: cloud evaporation (White & Long 1991) and thermal conduction (Cox et al. 1999). First, we consider the cloud evaporation model of White & Long (1991). According to this model, the SNR blast wave passes over the cold clouds, keeping them in the hot post-shock gas. X-ray emission arises from the gas evaporated from these shocked clouds. Secondly, we consider the radiative model of Cox et al. (1999), also called the 'fossil' conduction model. According to this model, the hot plasma in the interior of the remnant gradually becomes uniform by thermal conduction, and this is detectable as centrally brightened in X-rays.

We have studied the radial variations of the electron temperature and surface brightness profiles (see Fig. 3) to compare with these two models. We see that there is no strong radial temperature variation (∼0.06 keV), and this is consistent with the predictions of both evaporation and thermal conduction models. The observed surface brightness variation, which peaks at the centre ($\sim 1.26 \times 10^{-11}$ erg s^{-1} cm^{-2} arcmin^{-2}) and declines towards the outer region ($\sim 0.38 \times 10^{-11}$ erg s^{-1} cm^{-2} arcmin^{-2}), is consistent with the evaporation model. However, in the vicinity of this remnant, no molecular cloud or density gradient of the medium has yet been reported. This case is inconsistent with the predictions of both models. The young age ($\sim 4300 f^{1/2}$ yr) of the remnant, in other words the NEI condition of the plasma, cannot be explained by the thermal conduction model, which requires a collisional ionization equilibrium condition of the plasma. Therefore, considering all these facts, the centrally peaked X-ray emission of this remnant can be explained using the cloud evaporation model.

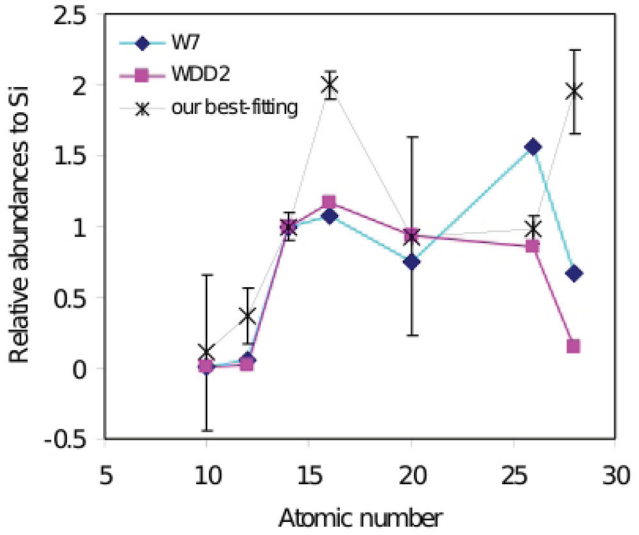

Figure 4. The best-fitting abundance ratios of Ne, Mg, Si, S, Ca, Fe and Ni relative to Si are shown by crosses. The predicted abundance ratios from the carbon deflagration (W7; Nomoto et al. 1997) model are shown by diamonds and those from the delayed detonation (WDD2; Nomoto et al. 1997) model are shown by squares.

5.3 Relative abundances in the ejecta

A Type Ia SN produces very small quantities of low-Z elements, such as Ne and Mg, and larger amounts of Si-group elements, such as S and Ca, and overabundant Fe and Ni, as in our case with G272.2−3.2. Therefore, we compare our best-fitting relative abundances with the predicted nucleosynthesis yield of the widely used W7 model and a delayed detonation (WDD2) Type Ia SN model (Nomoto et al. 1997), as given in Fig. 4.

Although the abundances of Ne, Mg and Ca relative to Si are almost consistent with both models, S and Ni relative to Si are higher than the values that both models predict. The value of Fe relative to Si is consistent with the WDD2 model, while it is much lower than the value that the W7 model predicts. The reason for the low value of Fe might be that the entire Fe-rich core has not yet been shocked, as is the case for SN 1006 (Yamaguchi et al. 2008), Tycho (Tamagawa et al. 2009) and G337.2−0.7 (Rakowski, Hughes & Slane 2001). Our results confirm that G272.2−3.2 has a Type Ia SN origin.

ACKNOWLEDGMENTS

AS is supported by a TÜBİTAK Post-Doctoral Fellowship. This work is supported by the Akdeniz University Scientific Research Project Management.

REFERENCES

Anders E., Grevesse N., 1989, Geochim. Cosmochim. Acta, 53, 197
Arnaud K. A., 1996, in Jacoby G., Barnes J., eds, ASP Conf. Ser. Vol. 101, Astronomical Data Analysis Software and Systems V. Astron. Soc. Pac., San Francisco, p. 17

Borkowski K. J., Lyerly W. J., Reynolds S. P., 2001, ApJ, 548, 820
Cox D. P., Shelton R. L., Maciejewski W., Smith R. K., Plewa T., Pawl A., Róyczka M., 1999, ApJ, 524, 179
Dickey J. M., Lockman F. J., 1990, ARA&A, 28, 215
Duncan A. R., Primas F., Rebull L. M., Boesgaard A. M., Deliyannis C. P., Hobbs L. M., King J. R., Ryan S. G., 1997, MNRAS, 289, 97
Greiner J., Egger R., 1993, IAU Circ. 5709
Greiner J., Egger R., Aschenbach B., 1994, A&A, 286, L35
Harrus I. M., Slane P. O., Smith R. K., Hughes J. P., 2001, ApJ, 552, 614
Ishisaki Y. et al., 2007, PASJ, 59, 113
Koyama K. et al., 2007, PASJ, 59, 23
Lopez L. A., Ramirez-Ruiz E., Huppenkothen D., Badenes C., Pooley D. A., 2011, ApJ, 732, 114
Masai K., 1984, Ap&SS, 98, 367
Mitsuda K. et al., 2007, PASJ, 59, 1
Morrison R., McCammon D., 1983, ApJ, 270, 119
Nomoto K., Iwamoto K., Nakasato N., Thielemann F.-K., Brachwitz F., Tsujimoto T., Kubo Y., Kishimoto N., 1997, Nucl. Phys. A, 621, 467
Park S., Lee J., Hughes J. P., Slane P. O., Burrows D. N., Mori K., Garmire G. P., 2009, Amer. Astron. Soc., 41, 695
Rakowski C. E., Hughes J. P., Slane P., 2001, ApJ, 548, 258
Tamagawa T. et al., 2009, PASJ, 61, 167
White R. L., Long K. S., 1991, ApJ, 373, 543
Winkler P. F., Hanson G. J., Phillips M. M., 1993, IAU Circ. 5715
Yamaguchi H. et al., 2008, PASJ, 60, 141

This paper has been typeset from a TEX/LATEX file prepared by the author.